

Iron Ore 2017

Paper Number: 56

Simulation investigation of flow patterns and feeder loads at hopper/feeder interface

J. Guo¹, A. W. Roberts², K. Williams³, M. Jones⁴, B. Chen⁵, J.Y. Guo⁶

1.

Research Associate, The University of Newcastle. Email: jie.guo@newcastle.edu.au

2.

Emeritus Professor, The University of Newcastle. Email: Alan.Roberts@newcastle.edu.au

3.

Associate Professor, The University of Newcastle. Email: Ken.Williams@newcastle.edu.au

4.

Professor, The University of Newcastle. Email: mark.jones@newcastle.edu.au

5.

Research Engineer, TUNRA Bulk Solids, Email: bin.chen@newcastle.edu.au

6.

Undergraduate, Central South University, Email: guo_jinyang@163.com

ABSTRACT

Numerical simulations using the Discrete Element Method (DEM) were carried out to investigate the flow patterns and stress field redistribution at the hopper and feeder interface. The influences of different filling heights, belt speeds and clearances between the hopper bottom and feeder surface on feeder loads were studied. Meanwhile, experiments were conducted by utilising wedged plane-flow hoppers with different configurations and horizontal feeders with various clearances. The simulation results were compared with theoretical values and experimental measurements. In terms of the cases presented in this study, simulation results reveal good agreements with experimental observations regarding the flow pattern. Being similar to the theoretical values, the simulations provide close predictions on vertical feeder loads for steady flow states, but they may show significant overestimations for initial states. Additionally, suggestions are given for relevant simulation parameters based on the comparisons shown in this investigation.

Keywords: hopper/feeder interface, flow patterns, feeder loads, numerical simulation, experimental comparison

INTRODUCTION

Feeders play an important role in bulk solids handling operations due to their extensive use for controlling the gravity flow of bulk solids from bins and stockpiles. To ensure efficient feeding, the hopper and feeders are designed as an integral unit. The interactions between hoppers and feeders have been investigated experimentally by Eckersley (1983), who noticed that the clearance between hoppers and feeders as well as the filling rate directly affected the feeder loads. The results showed that the fast filling leads to higher initial loads than the slow loading and larger clearances between the hopper and feeder result in lower initial loads on the feeder. However, there is still a shortage of knowledge regarding the hopper and feeder interface, especially for the pressure distribution along the hopper opening for both the initial and flow conditions. From a practical point of view, the vertical feeder loads are calculated based on the dimension of the middle point of the hopper outlet, which averages the variation of the hopper outlet due to the divergence angle. In this study, simulations of various hopper/feeder configurations were carried out to investigate the variations of the normal pressure along the hopper outlet. The relation between clearances, filling heights and feeder load distributions are also discussed in this paper based on the results of DEM simulations.

Relevant theories on feeder loads for both axisymmetric and plane-flow hoppers have been reviewed in the past by Roberts et al (Roberts, Ooms and Manjunath, 1984; Roberts, 2001a). The average vertical pressure at the hopper outlet is usually considered as the cause of vertical loads acting on feeders. It is derived from the force equilibrium analysis of horizontal slices. The vertical feeder load can be expressed mathematically by Equation 1 to 7 (Arnold, McLean and Roberts 1989; Jenike, 1977; McLean and Arnold, 1979). For convenience, a non-dimensional surcharge factor q is introduced. The vertical load acting on feeders is:

$$Q = p_{VO} \left(\frac{\pi}{4}\right)^m L^{1-m} B^{m+1} \quad (1)$$

$$q = \left(\frac{\pi}{4}\right)^m \frac{p_{VO}}{\gamma B} \quad (2)$$

$$K = \frac{P_n}{P_v} \quad (3)$$

$$p_n = \gamma K \left\{ \frac{h_o - z}{n-1} + \left[h_c - \frac{h_o}{n-1} \right] \left[\frac{h_o - z}{h_o} \right]^j \right\} \quad (4)$$

$$j = (m + 1) \left\{ K \left(1 + \frac{\tan \phi}{\tan \alpha} \right) - 1 \right\} \quad (5)$$

$$h_c = \frac{R}{\mu K_j} \left[1 - e^{-\mu K_j H/R} \right] + h_s e^{-\mu K_j H/R} \quad (6)$$

$$R = \frac{D}{2(1+m_c)} = \text{Characteristic Radius} \quad (7)$$

A general expression for the non-dimensional surcharge factor can be derived using Equation 2 to 4:

$$q = \left(\frac{\pi}{4}\right)^m \frac{1}{2(n-1)\tan\alpha} \left\{1 + [2(j-1)h_c \tan\alpha - D] \frac{B^{j-1}}{D^j}\right\} \quad (8)$$

Initial load case

With respect to the initial filling condition, by assuming the initial filling pressure distribution is hydrostatic according to Jenike's theory, the initial surcharge factor is obtained when $j = 0$ (Jenike, 1977; Jenike, 1964), as shown in Equation 9. Apart from this method, Equation 10 from McLean and Arnold (1979) is also used in the comparison of experimental and simulation results in this paper, in which $j = 0.3$.

$$q_i = \left(\frac{\pi}{4}\right)^m \frac{1}{2\tan\alpha} \left[\frac{D}{B} + \frac{2h_c \tan\alpha}{B} - 1 \right] \quad (9)$$

$$q_i = \left(\frac{\pi}{4}\right)^m \frac{1}{2\tan\alpha} \left[\frac{D}{B} + \frac{2h_c \tan\alpha}{D} - 1 \right] \quad (10)$$

Flow case

McLean's and Arnold's method

McLean and Arnold adopted the maximum ratio of normal wall pressure p_n and average vertical pressure in bins p_v , called K value, to obtain the non-dimensional surcharge factor for the flow case (Arnold, McLean and Roberts, 1989; McLean and Arnold, 1979).

$$q_f = \frac{1}{4} \left(\frac{\pi}{3}\right)^m \frac{1}{\tan\alpha} \left[\frac{Y}{X-1} \left(\frac{1+\sin\delta \cos 2\beta}{\sin\alpha} \right) (\tan\alpha + \tan\emptyset) - \frac{1}{1-m} \right] \quad (11)$$

$$\beta = \frac{1}{2} \left[\emptyset + \sin^{-1} \left(\frac{\sin\emptyset}{\sin\delta} \right) \right] \quad (12)$$

$$X = \frac{2^m \sin\delta}{1-\sin\delta} \left[\frac{\sin(2\beta+\alpha)}{\sin\alpha} + 1 \right] \quad (13)$$

$$Y = \frac{[2(1-\cos(\beta+\alpha))]^m ((\beta+\alpha))^{1-m} \sin\alpha + \sin\beta \sin^{1+m}(\beta+\alpha)}{(1-\sin\delta) \sin^{2+m}(\beta+\alpha)} \quad (14)$$

Roberts' method

An alternative approach to determine the flow surcharge factor was proposed by Roberts (Arnold, McLean, Roberts, 1989), who used a pressure multiplier for the average vertical pressure at the hopper outlet, as shown in Equation 15 and 16. The K value which is required to calculate j is given by Equation 18.

$$k_{Fm} = \frac{1+\sin\delta}{1-\sin\delta \cos 2(\beta+\alpha)} \quad (15)$$

$$p_{vod} = k_{Fm} p_{vo} \quad (16)$$

$$q_f = k_{Fm} \left(\frac{\pi}{4}\right)^m \left\{ \frac{1}{2(j-1)\tan\alpha} + \left[\frac{h_c}{D} - \frac{1}{2(j-1)\tan\alpha} \right] \left[\frac{B}{D} \right]^{j-1} \right\} \quad (17)$$

$$j = (m+1) \left\{ K \left(1 + \frac{\tan\emptyset}{\tan\alpha} \right) - 1 \right\}$$

$$K = \frac{2(1+\sin\delta\cos2\beta)}{2-\sin\delta(1+\cos2(\beta+\alpha))} \quad (18)$$

Reisner's method

Taking into consideration that the stress field at the hopper outlet will change due to the operation of feeders, Reisner suggested two methods for feeder load calculations which are based on the normal wall pressure and major consolidation stress, respectively (Reisner, Eisenhart and Rothe, 1971). The approach based on the normal wall pressure is used to compute the load on belt feeders, apron feeders and table feeders. The method based on the major consolidation stress is implemented to determine the load on vibratory feeders. Earlier results (Roberts, 2001a) suggested that this method based on the major consolidation stress can also be used to predict the loads for belt feeders.

$$q_{f\sigma_1} = \left(\frac{\pi}{4}\right)^m \frac{Y(1+\sin\delta)}{2(X-1)\sin\alpha} \quad (19)$$

Roberts Alternative method

Apart from the methods mentioned previously, another method was discussed by Roberts (1998). It assumed that the average vertical pressure p_{vod} for designing was equal in magnitude to the major consolidation stress σ_1 at the hopper feeder interface. Instead of utilising the pressure multiplier in Equation 15, the surcharge factor is calculated by Equation 17 substituting the pressure multiplier in Equation 25.

$$P_{vod} = \sigma_1 = C_2 p_v \quad (20)$$

$$C_2 = \frac{k_{hf}(1+\sin\delta)}{1+\sin\delta\cos2\eta} \quad (21)$$

$$k_{hf} = \frac{2(1+\sin\delta\cos2\eta)}{2-\sin\delta(1+\cos2(\eta+\alpha))} \quad (22)$$

Then

$$C_2 = \frac{2(1+\sin\delta)}{2-\sin\delta(1+\cos2(\eta+\alpha))} \quad (23)$$

$$K_{Fm} = C_2 \quad (24)$$

$$k_{Fm} = \frac{2(1+\sin\delta)}{2-\sin\delta(1+\cos2(\eta+\alpha))} \quad (25)$$

It is noted that this method adopts the same assumption as Reisner's method. Both of these approaches are on the basis of the major consolidation stress at the hopper bottom. However, there is a slight difference between the results obtained from Reisner's method and this alternative method. The variation results from the different methods used to calculate the consolidation stress, the former is based on the circular arch stress field analysis and the latter is based on the horizontal slice stress field analysis (Roberts, 2010).

SIMULATION INVESTIGATION

Case 1

In order to investigate the influence of the feeder operation on flow patterns and feeder loads in an integrated hopper/feeder unit, a series of simulations were conducted. The DEM software package used for this simulation is Rocky, Version 2.3.0 (Granular Dynamics International, USA), which applies a hysteresis linear spring model for the normal force interactions and an elastic-frictional force model in the tangential direction by default. Further information on the model can be found in the software reference.

The geometric model of the mass-flow bin and feeder used to carry out these DEM simulations is illustrated in Figure 1. This wedged plane-flow hopper was equipped with vertical skirtplates. They featured a tapered outlet opening with a 4° divergence angle and a 3.5° release angle. The outlet widths at the rear end and at the front end were 40mm and 160mm respectively. The clearances between hopper and feeder were 55mm

at the front hopper outlet and 5mm at the rear end. The length of the outlet is 800mm. It is noted that there was an alteration of the inclined hopper walls which resulted in a change of the hopper half angle from 20° to 26°. The dimensions of this model were identical with the experimental validation setup in the subsequent section.

Figure 1: Geometry model for DEM analysis – Case 1

Figure 2: Initial filling condition

The modelling parameters that were selected for this simulation are listed in Table 1. The particle's rolling resistance was selected according to the experimental angle of repose of 35°. Because the load distributions on the feeder for the initial filling and steady flow conditions were of interest, the same amount of material by weight was implemented in all simulations. In the simulation, the belt feeder was set to operate at a constant speed after the material filling process was completed. The acceleration of the feeder during start-up was neglected, as it would not affect the vertical load distribution for the two aimed conditions.

Table 1: Modelling parameters

Flow patterns

Figure 2 illustrates the initial filling state of the model hopper, featuring a coloured layer of material. Once the belt movement was initiated, the material flowed faster in two areas, at the rear end and in the middle region respectively. The S shape of the top surface and the coloured layer of material appeared significantly with time as displayed in Figure 3. Full discharge of the material at the rear end was accomplished earlier than at the front end of the hopper outlet, as shown in Figure 3 at 41.45s. However, considering the difference in particle sizes used in both simulations and experiments, further study investigating the influence of the material particle size on observed flow patterns in simulations was also conducted.

Figure 3: Flow patterns during discharge at different points of time

Load analysis

The vertical load distribution on the feeder was analysed and the results are shown in Figure 4a. The red and blue lines represent the normal force distributions for the initial condition and steady flow condition respectively. An increase of the normal load for both the initial and flow conditions shows along the hopper length from the rear end to the front end due to the increased hopper outlet opening. It can be seen that the initial normal load on the feeder is much larger than the load for the flow case. It should be noted that the normal force distribution differs from the pressure distribution shown in Figure 5 and Figure 6, as the latter depends on the shape of the outlet. More details will be addressed in the following discussion.

To investigate the influences of the particle size and belt speed on feeder loads, the normal feeder load distributions regarding variable parameters are compared in Figure 4. Figure 4a and Figure 4b reveal the normal force comparison between two different belt speeds but with the same particle size, whereas Figure 4a and Figure 4c demonstrate the comparison between different simulated particle sizes but with the same belt speed. It seems that, for both initial and steady flow conditions in these three cases, the normal forces distribute in the same trend regardless of different particle sizes and belt speeds. The change of the belt speed and particle size in the studied range leads to negligible differences on feeder loads.

The normal pressure distributions are compared between simulation and theoretical results in Figure 5 for the initial case and in Figure 6 for the flow case. The normal pressure is computed from the normal force divided by the material and feeder contacting area. This contacting area is dependent on many factors, such as the shape of the outlet, the presence of the skirtplates and the clearance between the hopper and feeder. With skirtplates at the hopper outlet, the material at the hopper and feeder interface would be constrained instead of free flowing. In this study, the weight of the material between the hopper bottom and feeder surface was taken into account when calculating normal forces on the feeder.

In Figure 5, it can be seen that the method proposed by Arnold and McLean (1979) provides a relatively lower pressure distribution curve comparing with the Jenike method, and the latter matches the three simulation results quite well except at the rear and front ends. There are significant pressure increases approaching the front and rear end boundaries for the simulation results. It is believed that this is due to the effect of the boundary transition of the hopper zone and the feeder zone, for which the theories have neglected. For the flow case shown in Figure 6, the simulation results are in good agreement with the result based on the Reisner method, which offers the highest prediction for feeder loads among the compared theories.

- (a) Belt speed = 0.35 m/s, particle diameter = 0.01 m
- (b) Belt speed = 0.05 m/s, particle diameter = 0.01 m
- (c) Belt speed = 0.35 m/s, particle diameter = 0.005 m

Figure 4 Vertical loads on the feeder at varying belt speeds and particle sizes

Figure 5 Normal pressure distribution comparison between simulation and theoretical results for initial case

Figure 6 Normal pressure distribution comparison between simulation and theoretical results for flow case

Additionally, two more scenarios for the same geometric model were simulated, one featuring a higher initial filling level and one featuring a larger clearance between the hopper and feeder. The results are shown in Figure 7, in which the red and blue lines represent the initial and flow cases respectively. In the case of a 0.75m filling height, the filling level is considerably above the hopper transition area. In contrast, the filling level of the first scenario with 200kg material is generally below the transition area as shown in Figure 3. In the case of the initial filling height being below the transition area, the level where the free loading surface locates is deemed to be the actual transition with no surcharge pressure.

By way of comparison, the filling height can affect the initial vertical load in both its magnitude and tendency, whereas it does not have a significant influence on the load distribution for the flow condition. For initial conditions, the vertical load in the hopper section is often assumed to be hydrostatic so that it is susceptible to the initial filling height, which contributes to the load distribution differences shown in *Figure 7a* and *Figure 7b*.

- (a). clearance between hopper outlet and feeder=55mm, filling height=450mm
- (b). clearance between hopper outlet and feeder =55mm, filling height=750mm
- (c). clearance between hopper outlet and feeder =120mm, filling height=450mm

Figure 7: Vertical loads on feeder at varying filling heights and clearances

Due to the increased clearance of 120mm between the hopper and feeder, a substantial amount of material discharged from the hopper onto the belt, which initializes the passive stress state in the hopper for initial filling conditions. The development of an arched stress field can reduce the vertical loads significantly. This cushioning effect is shown in Figure 7c, which has been reported before by Roberts et al. (Roberts, Ooms and Manjunath, 1984). There are other methods to facilitate the formation of the arched stress field for the initial filling condition, such as increasing the clearance between the hopper and feeder or lowering the feeder after filling. This will be discussed in the subsequent section.

The distinguishable increase of the normal force approaching the front end is in the same order as the one in Figure 7a. The reason that the vertical load in this region is not reduced is due to the increased weight of the significant amount of material discharged at the front end. It is noted that the steady flow load generally increases because of the increased depth of the material bed above the feeder.

Case 2

To investigate the influences of skirt plates and changing configurations on flow patterns and feeder loads, the second series of simulations were conducted. A wedged plane-flow hopper with one constant hopper

angle of 20° and without skirtplates was studied for this case. The rear end and the front end of the hopper outlet were 130mm and 166mm respectively. The release angle and the length of the outlet remained the same as Case 1, which lead to a smaller divergence angle of 1.26°. The modelling parameters were identical to the ones listed in Table 1. The geometry of the simulation model is shown in Figure 8.

Figure 8 Geometry model for DEM analysis - Case 2

Figure 9 Initial filling condition

Flow patterns

Figure 10 Flow patterns during discharge at different points of time

Figure 9 illustrates the initial filling status of the material for the flow pattern study. The simulated flow pattern is demonstrated in Figure 10. It can be seen that there is one rapid flow channel at the rear end of the hopper outlet. With the flow of the material at the front, material layers slowly mix. The material at the rear finishes discharging first, which is shown by the last image in Figure 10.

Different draw-down profiles of the material are observed in Figure 3 and Figure 10 due to the change of the hopper configuration. Figure 3 reveals two fast flow channels, which represents a more uniform draw-down. According to the analysis in the reference (Roberts, 2001b), it is impossible to achieve an absolutely uniform draw-down for which the material surface remains completely level during discharge. The fast discharge channel in the middle of the hopper outlet in Figure 3 relieves the possible shear force between the material and the belt to some extent. It slows down the belt wear occurring at the rear end of the outlet. Therefore it is suggested that the introduction of a special hopper configuration can result in a more satisfactory draw-down profile in an hopper and feeder unit for some cases.

Load analysis

- (a) *Belt speed=0.05m/s*
- (b) *Belt speed=0.15m/s*
- (c) *Belt speed=0.25m/s*

Figure 11: Vertical loads on feeder at varying belt speeds

The simulation results with various belt speeds involved are compared in Figure 11. It is shown that the influence of belt speeds is not apparent on feeder load distributions. Figure 11 demonstrates that the vertical loads for both initial and flow conditions distribute more evenly without an obvious decreasing or increasing trend comparing with Case 1 in Figure 4. The reason is that, due to the absence of the vertical skirtplates, the material at the interface can flow freely out of the outlet to develop a relatively uniform load.

The pressure distributions are compared with theoretical results in Figure 12 and Figure 13. For the initial condition, the calculations based on the Jenike method and the Arnold and McLean method are identical as the surcharge pressure is zero. The pressures from simulations fluctuate along the theoretical estimation line. The overall load for each case is quite close to the theoretical feeder load. For the flow condition in Figure 13, the Roberts alternative method provides the highest pressure distribution whereas the Arnold and McLean method offers the lowest pressure distribution. The simulation results generally lie in between these theoretical pressure distribution lines.

Figure 12 Normal pressure distribution comparison between simulation and theoretical results for initial case

Figure 13 Normal pressure distribution comparison between simulation and theoretical results for flow case

The influence of increasing clearance

The influence of lowering the feeder during consolidation on feeder loads is investigated by corresponding simulations as shown in Figure 14 and Figure 15.

For the initial condition illustrated in Figure 14, the experimental feeder loads show an initial decrease with the increased clearance due to the development of the arched stress field in the hopper. A large proportion of the vertical stress was shifted and supported by the hopper walls in this case. With the further increase of the clearance after 30mm, the feeder loads start to rise. This is due to the increased amount of material remaining between the hopper outlet and the feeder surface. The weight of the material was carried by the feeder directly which gave rise to the increase of the feeder loads. The simulations do not show good agreement with experimental measurements, which overestimate the feeder loads for the cases with 0mm and 20mm clearances and underestimate the feeder load for the case with 40mm clearance. However, as for the cases with 10mm and 30mm clearances, the simulation results can provide close predictions. Further investigation is needed.

Figure 14: Comparison of the vertical feeder loads at different Clearances for initial condition

Figure 15: Comparison of the vertical feeder loads at different Clearances for flow condition

With regard to the flow condition shown in Figure 15, the feeder loads do not vary significantly with the increase of the clearance. A slight increase is noticed by comparing the case with 0mm clearance and the case with 40mm clearance. In this study, only the cases with 0mm and 40mm clearances were validated by experiments so that direct comparisons are limited for these two cases. Figure 15 shows that simulation results for flow conditions generally demonstrate a good agreement with the experimental results in terms of the studied cases.

EXPERIMENTAL VALIDATION

To validate the simulation results, two series of experiments were carried out based on the two simulation cases. The exact hopper and feeder configurations were implemented as shown in Figure 1 and Figure 8.

Case 1

The flow patterns obtained from the simulation were compared with the experimental flow patterns. Based on the configuration shown in Figure 1, a coloured material layer was inserted above the transition plane between the two hopper half angles and the flow patterns were recorded by a high speed camera.

Figure 16: Observed flow patterns: a) Initial position of marked material layer b) 'U' shaped flow pattern at front hopper wall during discharge c) 'S' shaped top surface from side view during discharge d) 'S' shaped flow pattern of marked layer from side view during discharge e) Top view of hopper in the middle of discharge f) Top view of hopper at the end of discharge

Figure 16 shows the flow patterns observed in the hopper during discharge from different perspectives. Figure 16a demonstrates the position of the marked layer. A 'U' shaped pattern was observed at the front hopper wall (Figure 16b), which was a typical flow pattern for mass-flow hoppers with the bulk material in the centre flowing faster than the material next to the hopper walls.

From the side view of the hopper, an 'S' shape top surface profile emerged during flow (Figure 16c). The yellow line in Figure 16c illustrates this vividly. Figure 16d shows that the coloured layer of material followed the same flow pattern as the top layer of material. A further yellow tracing line marks the established flow pattern. To the author's knowledge, this 'S' shape of flow pattern was not reported in any other feeder study before. It may correlate with the special arrangement of the different hopper wall angles as discussed

precisely. According to the feeder draw-down theory suggested by Arnold et al (Arnold, McLean, Roberts, 1989), the top surface profile can be predicted, which will be published later along with further study.

Associated with these 'S' profiles, two fast mass-flow 'channels' were observed from the top view of the hopper (Figure 16e and Figure 16f). One possible explanation for this phenomenon is that two mass-flow zones established based on the respective hopper half angle. At each location, the majority of the hopper wall was made up of one angle. In the slow flow regions, the alteration of the hopper half angle from 20° to 26° disturbed the flow pattern formed at the upper section based on the 20° hopper half angle. This observation was in good agreement with the phenomenon illustrated in the simulations.

Figure 17 Comparison of the vertical feeder loads at different belt speeds for both initial and flow condition

The simulation results are also compared with the experimental and theoretical results in magnitude in Figure 17. The total initial loads from simulations are close to the theoretical values but larger than the experimental result. In terms of flow conditions, the Reisner method and the Roberts alternative method as well as the simulations can provide appropriate predictions for the feeder load, whereas the Arnold and McLean method and the Roberts original method underestimate the feeder load.

It is noted that the simulations showed minor variations of feeder loads with respect to different particle sizes and belt speeds. The scenario with the smaller particle size offered a relatively lower value on feeder loads comparing with larger particle sizes, which meant a less conservative result. From a practical point of view, these differences are negligible.

Case 2

Experimental studies were also undertaken using the same setup in Figure 8 with one constant hopper wall angle to corroborate the simulation findings for Case 2.

Figure 18: The top view of the flow patterns: a) the earlier time during discharge b) the later time during discharge

The flow patterns observed in these experiments are shown in Figure 18. The material flowed faster at the rear end and it turned out to be the only rapid flow area inside the hopper. The fast flow area started to appear a few seconds after the discharge initialized, as shown in Figure 18a. The material at the front end flowed down slowly and the top layer of the material slid backwards to a certain extent. It is a well-known flow pattern in practice and related to the moving direction of the feeder. This is because that, at the rear end, there is always clearance for the material to discharge as the bottom material is transported out and moving forwards. A long and thin flow channel along the length of the outlet emerged in the middle as indicated in Figure 18b. It suggested the significant mass-flow discharge occurring in this area. The experimental observations validated the flow patterns shown in simulations.

The disparity of the flow patterns within these two different plane-flow hoppers in Case 1 and Case 2 demonstrated the influence of the hopper shape on flow patterns during discharge. It delivered a hint that a properly designed plane-flow hopper with special configuration may lead to a relatively uniform draw-down by generating more rapid flow channels.

Figure 19: Comparison of the vertical feeder loads at different belt speeds for both initial and flow condition

The experimental and theoretical results are also compared with simulation results in Figure 19. For the initial case, which is represented by blue bars, the simulation results and theoretical results are in similar order but all overestimate the feeder loads. For the flow case, which is shown by red bars, the simulation results provide quite reliable predictions for the feeder loads. The theoretical calculations based on the Reisner method and the Roberts alternative method are in good agreement with the experimental results with reasonable margins.

CONCLUSION

Based on the cases investigated in this paper, the simulations conducted through Rocky can provide good indications regarding flow patterns in a hopper and feeder unit. The alteration of the hopper half angle in an integrated hopper and feeder unit can have significant influences on the flow patterns, which also means a relatively uniform draw-down can be achieved by an optimum hopper design. The draw-down profile can be predicted by simulations which have been presented in this paper or calculated by theories, however, the latter will be based on some assumptions of the stress and velocity fields at the hopper and feeder interface. Further details will be addressed in a separate paper.

The predictions for feeder loads by simulations for the flow case are in good agreement with the experimental measurements. However, the overestimation exists for feeder loads for the initial case. The feeder load distributions can be affected by many factors, such as the hopper configuration, the presence of the skirt plates, the initial filling height and the clearance between the hopper and feeder. The initial feeder loads can be significantly decreased by lowering the feeder after loading due to the development of the arched stress field in the hopper. However, an appropriate final clearance has to be controlled to avoid an increase of the feeder loads due to the weight of the material flowing out of the hopper.

Simulation results show that the feeder loads for both initial and flow cases are not sensitive to the belt speed. Additionally, the particle sizes have slight influences on feeder loads. The simulations, which utilised a smaller particle size, lead to a lower prediction for feeder loads for both initial and flow conditions, however, the differences may be ignored. Faster belt speeds and larger particle sizes can accelerate the simulation process to some extent. Therefore, to achieve effective simulations, it is wise to investigate the sensitivities of the input parameters for desired output parameters.

Among the various theories compared with experimental results, the feeder loads for initial conditions are considerably overestimated by both the Jenike method and the Arnold and McLean method. In terms of flow conditions, the Reisner method and the Roberts alternative method based on the major consolidation stress provide quite accurate predictions for feeder loads.

NOTATION

P_{v0} = Average vertical pressure at hopper outlet (Pa)

L = Hopper outlet length (m)

B = Hopper outlet width or diameter (m)

q = Non-dimensional surcharge factor

K = ratio of p_n/p_v for hopper

p_n = normal wall pressure (Pa)

p_v = average vertical pressure (Pa)

γ = bulk specific weight (N/m³)

h_0 = distance from apex to the transition of hopper (m)

z = depth coordinates from hopper transition (m)

h_c = surcharge head acting at transition of cylinder and hopper (Pa*m³/N)

m = symmetry factor, $m = 0$ for plane-flow hopper, $m = 1$ for axi-symmetric or conical hopper

α = hopper half angle (°)

φ = wall friction angle (°)

$m_c = 0$ for long rectangular cylinder; $m_c = 1$ for square or circular cylinder

$\mu = \tan\phi$ coefficient of wall friction

k_j = pressure ratio in Janssen equation

H = the head of bulk solid in cylinder (m)

h_s = bin surcharge head (m)

δ = effective angle of internal friction ($^\circ$)

REFERENCES

Arnold, P C, McLean, A G and Roberts, A W, 1989. *Bulk Solids: Storage, Flow and Handling*. The University of Newcastle Research Associates Ltd., 2nd Edition, 3rd Printing.

Eckersley, D, 1983. Interactive Rolls of Bins and Feeders. B.E. Thesis, The University of Newcastle, Australia.

Jenike, A W, 1964. *Storage and Flow of Solids*. Bul.123, Utah Engng. Exper. Station, University of Utah.

Jenike, A W, 1977. Load assumptions and distributions in silo design. Paper presented at Conference on Construction of Concrete Silos, Oslo, Norway, January.

McLean, A G and Arnold, P C, 1979. A simplified approach for the evaluation of feeder loads for Mass-flow Bins. *Journal of Power and Bulk Solids Technology*, 3(3): 25-28.

Reisner, A and Eisenhart Rothe M V, 1971. *Bins and Bunkers for Handling Bulk Materials*. Trans. Tech. Publications, Germany.

Roberts, A W, Ooms, M and Manjunath, K S, 1984. Feeder load and power requirements in the controlled gravity flow of bulk solids from mass-flow bins. *Transactions of Mechanical Engineering*, 9(1): 49-61.

Roberts, A W, 1998. *Basic Principles of Bulk Solids, Storage, Flow and Handling*. Centre for Bulk Solids and Particulate Technologies, The University of Newcastle, Australia.

Roberts, A W, 2001a. An overview of feeder design focusing on belt and apron feeders. *Bulk Solids Handling*, 21(1):13-24.

Roberts, A W, 2001b. Feeders and transfers - recent developments. *Transactions of Mechanical Engineering*, 25(1): 73-91.

Roberts, A W, 2010. Review of mass-flow hopper design with respect to stress fields and surcharge loads. *Particuology*, 8(6):591-594.

FIGURES

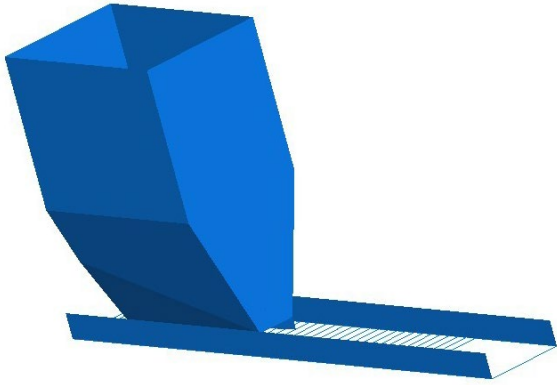


Figure 1: Geometry model for DEM analysis – Case 1

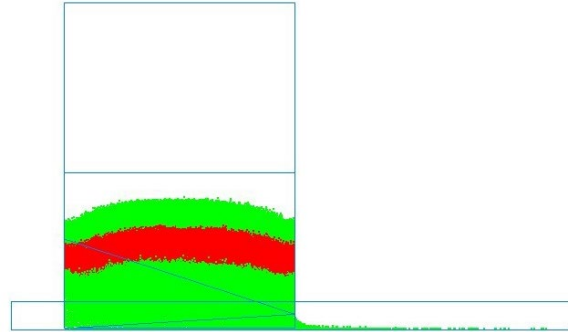


Figure 2: Initial filling condition

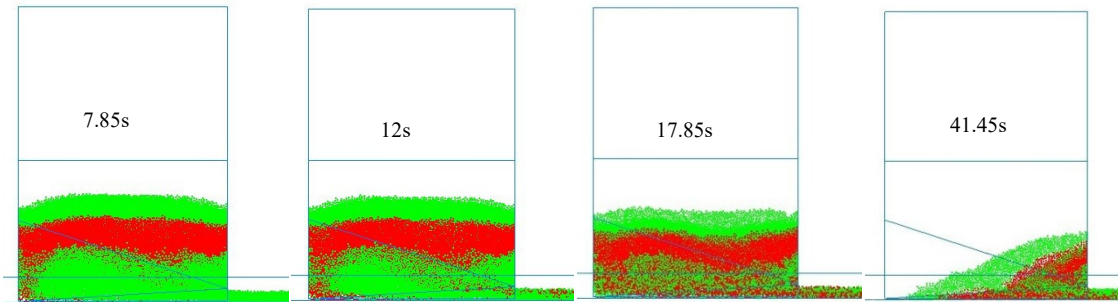
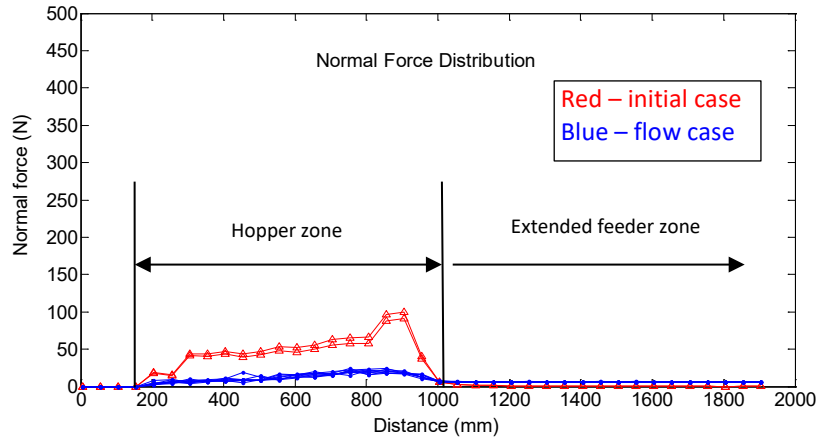
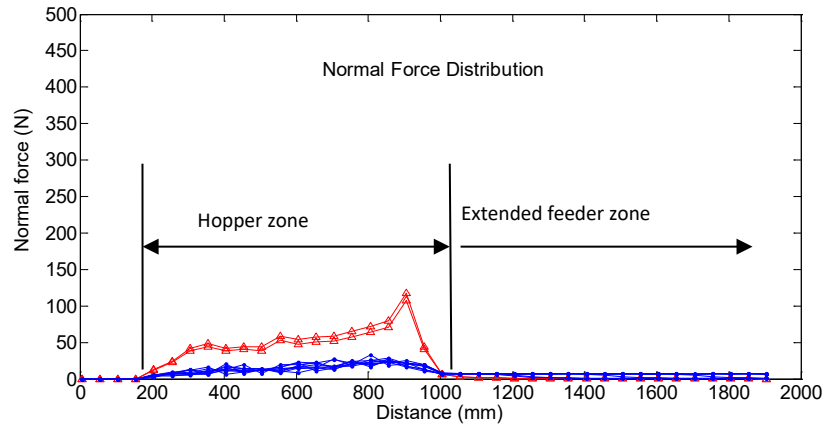


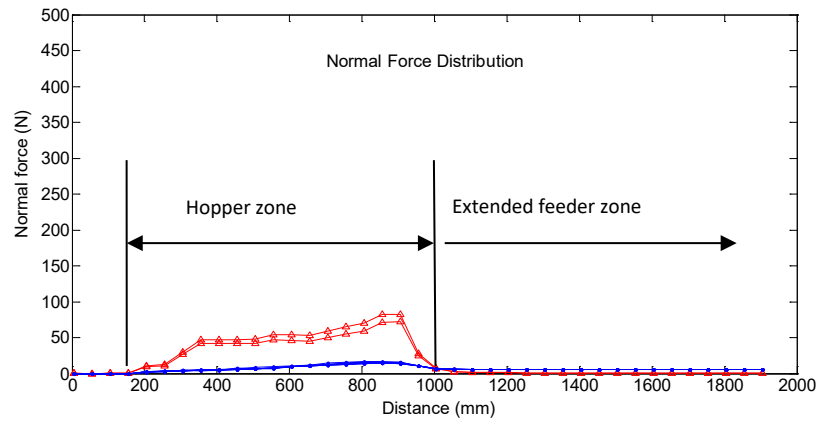
Figure 3: Flow patterns during discharge at different points of time



(a) Belt speed = 0.35 m/s, particle diameter = 0.01 m



(b) Belt speed = 0.05 m/s, particle diameter = 0.01 m



(c) Belt speed = 0.35 m/s, particle diameter = 0.005 m

Figure 4 Vertical loads on the feeder at varying belt speeds and particle sizes

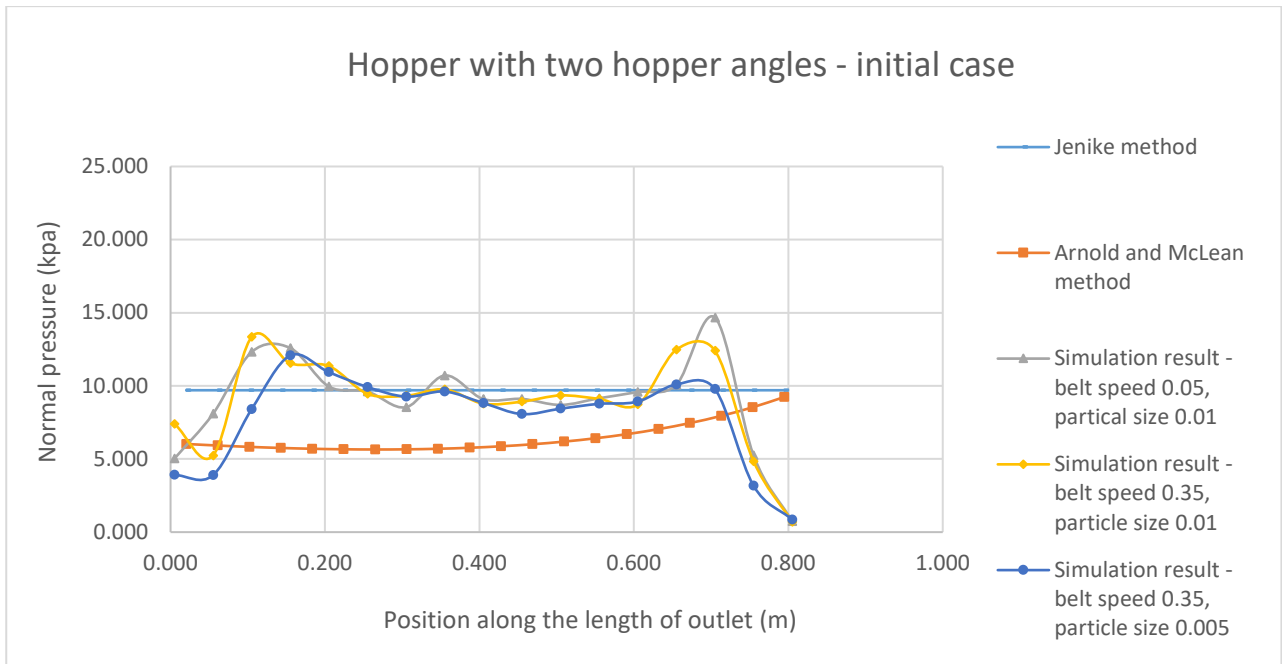


Figure 5 Normal pressure distribution comparison between simulation and theoretical results for initial case

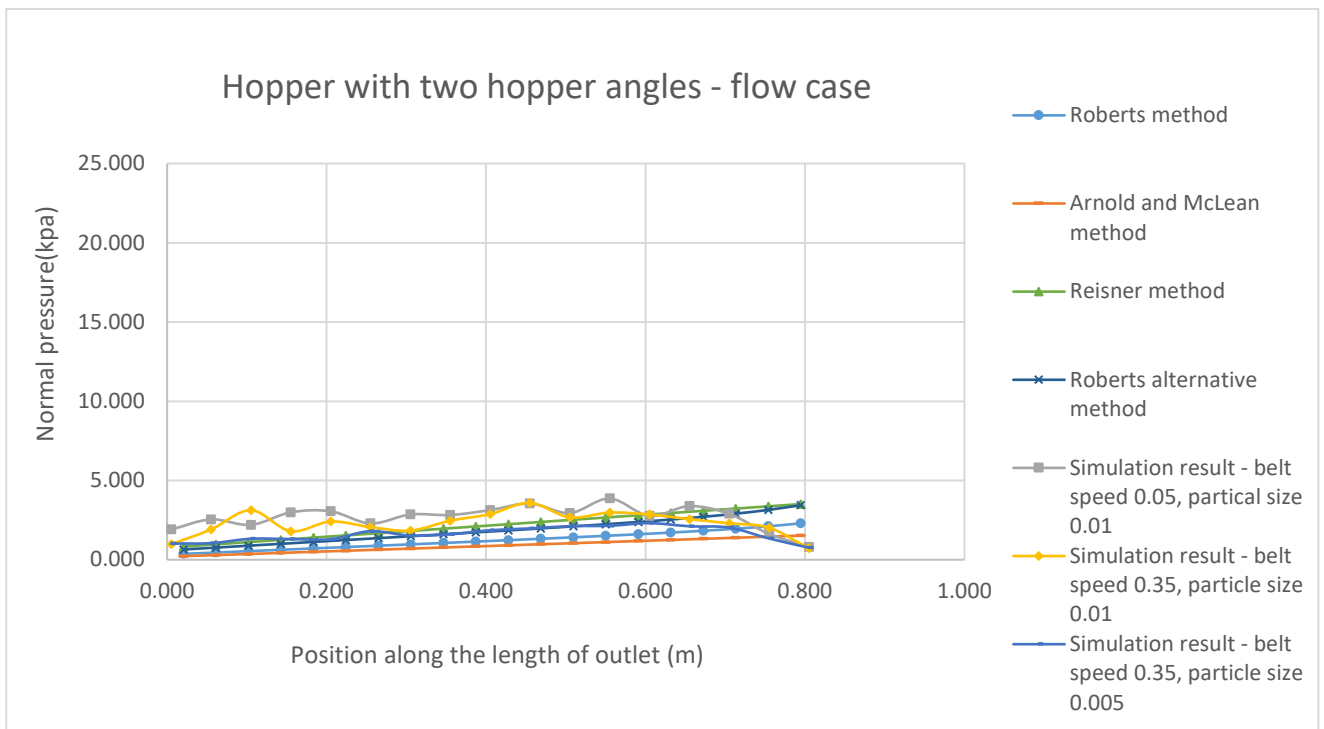
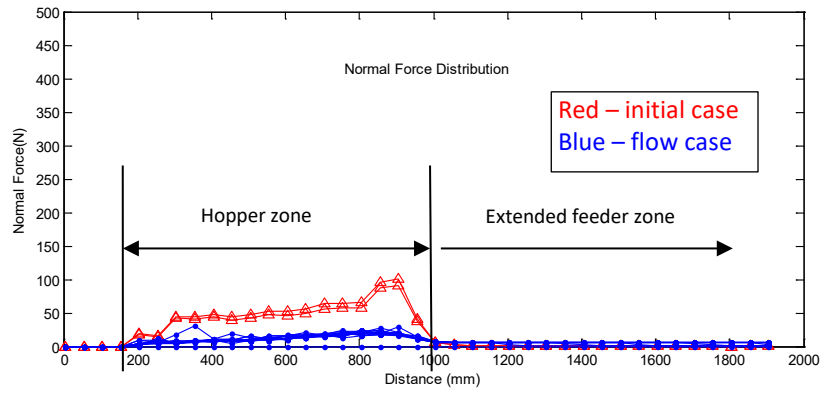
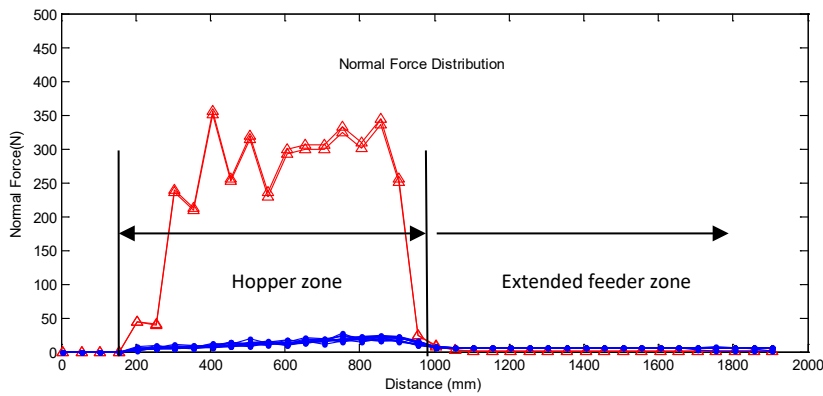


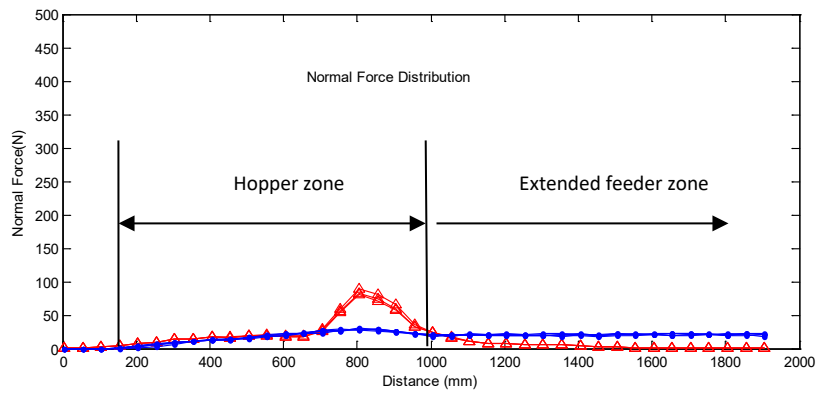
Figure 6 Normal pressure distribution comparison between simulation and theoretical results for flow case



a. clearance between hopper outlet and feeder=55mm, filling height=450mm



b. clearance between hopper outlet and feeder =55mm, filling height=750mm



c. clearance between hopper outlet and feeder =120mm, filling height=450mm

Figure 7: Vertical loads on feeder at varying filling heights and clearances

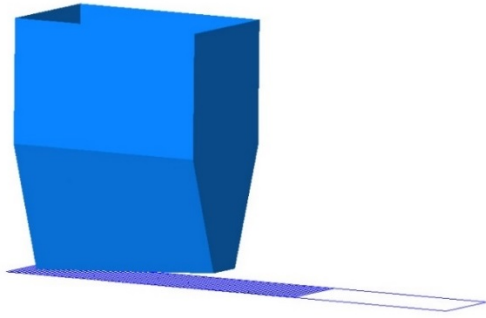


Figure 8 Geometry model for DEM analysis - Case 2

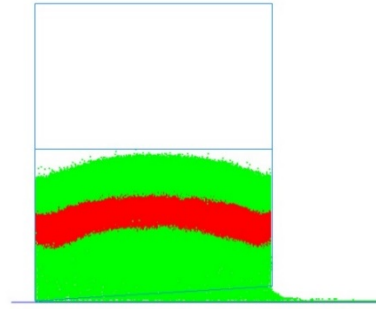


Figure 9 Initial filling condition

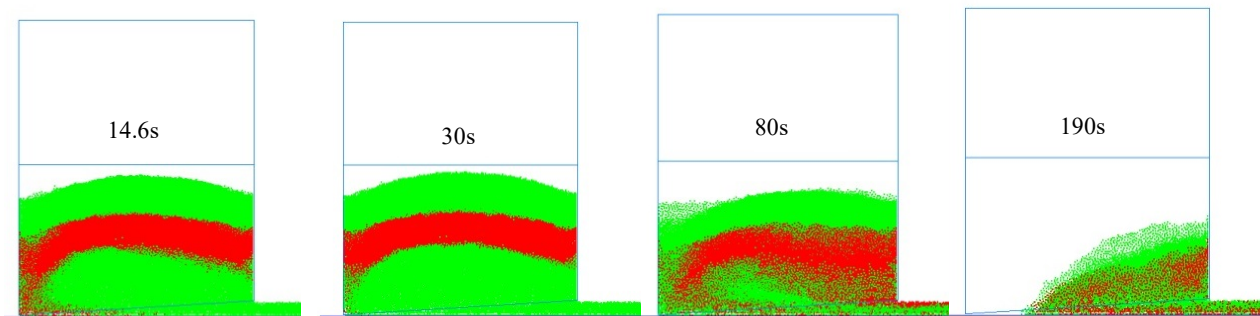
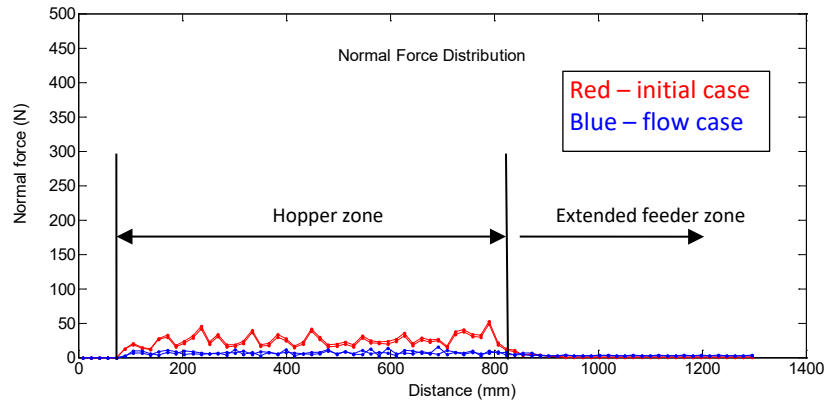
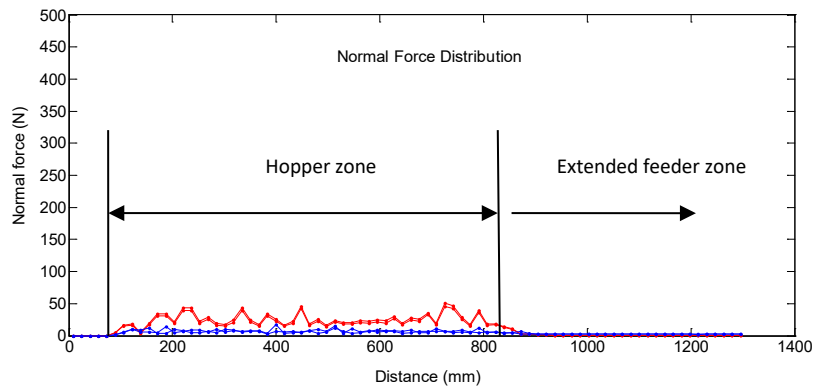


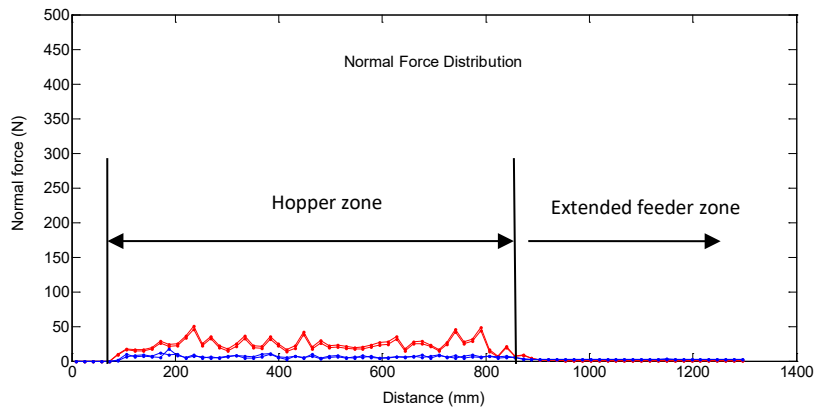
Figure 10 Flow patterns during discharge at different points of time



(a) Belt speed=0.05m/s



(b) Belt speed=0.15m/s



(c) Belt speed=0.25m/s

Figure 11: Vertical loads on feeder at varying belt speeds

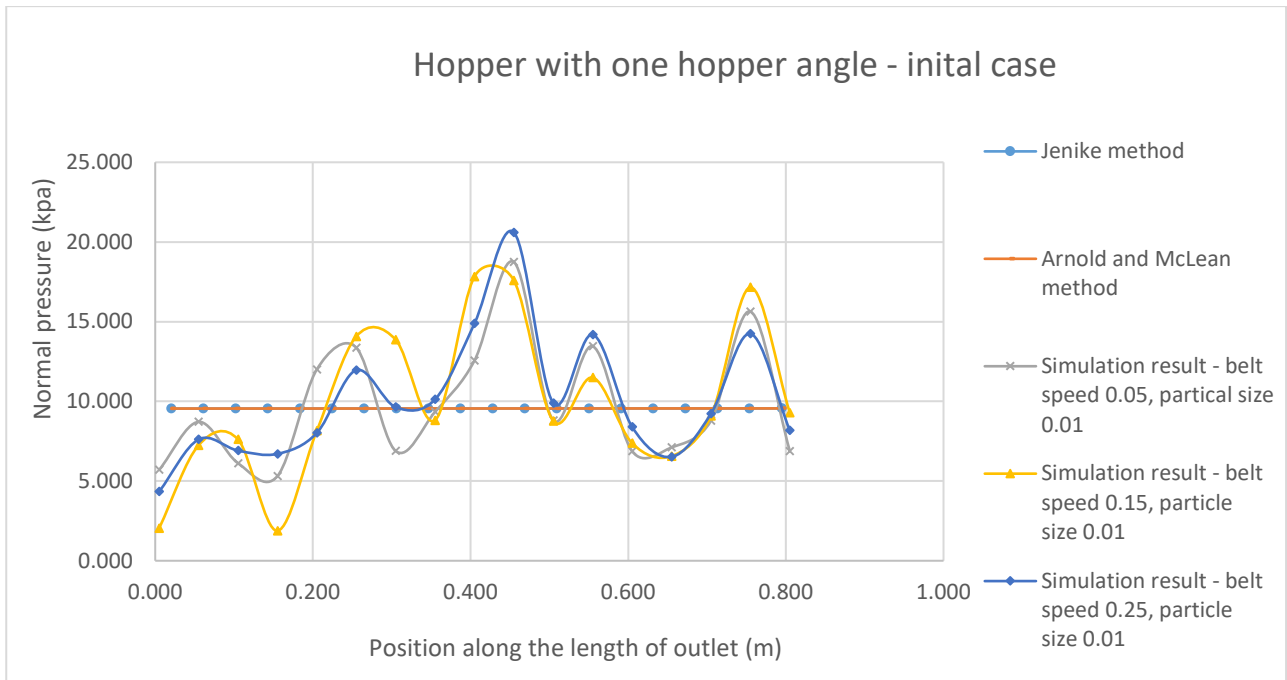


Figure 12 Normal pressure distribution comparison between simulation and theoretical results for initial case

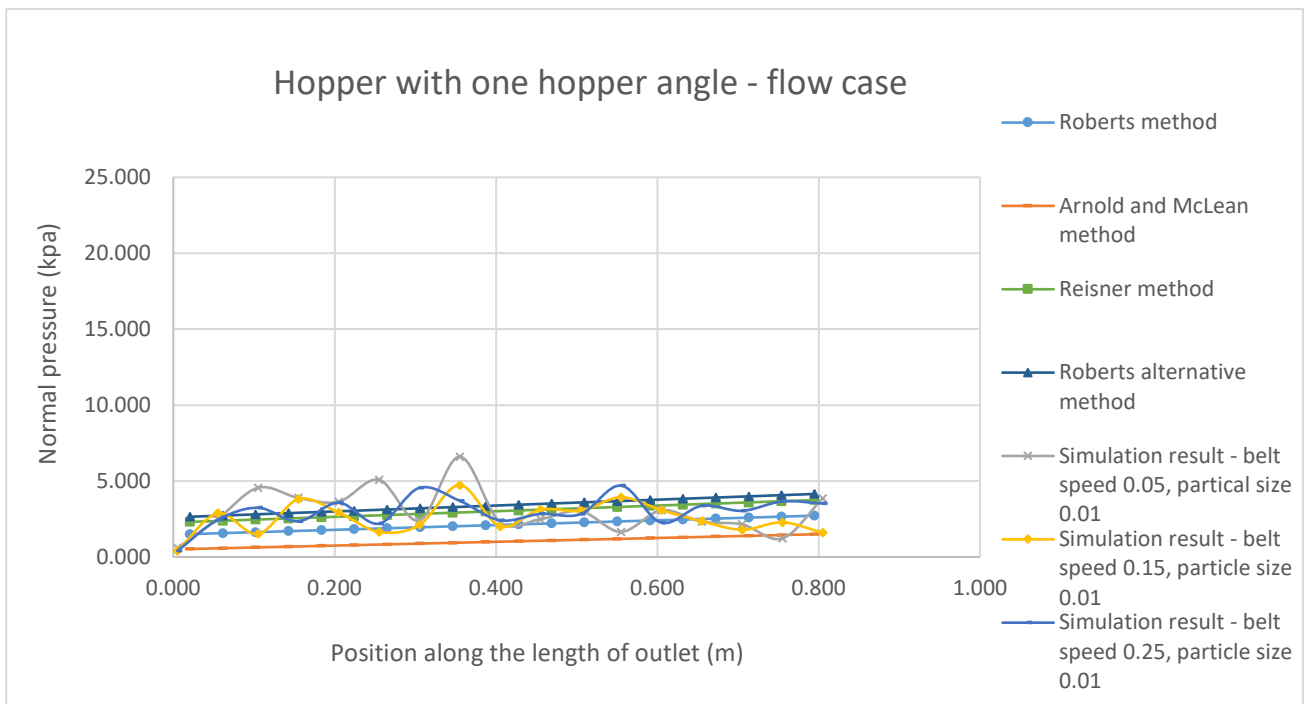


Figure 13 Normal pressure distribution comparison between simulation and theoretical results for flow case

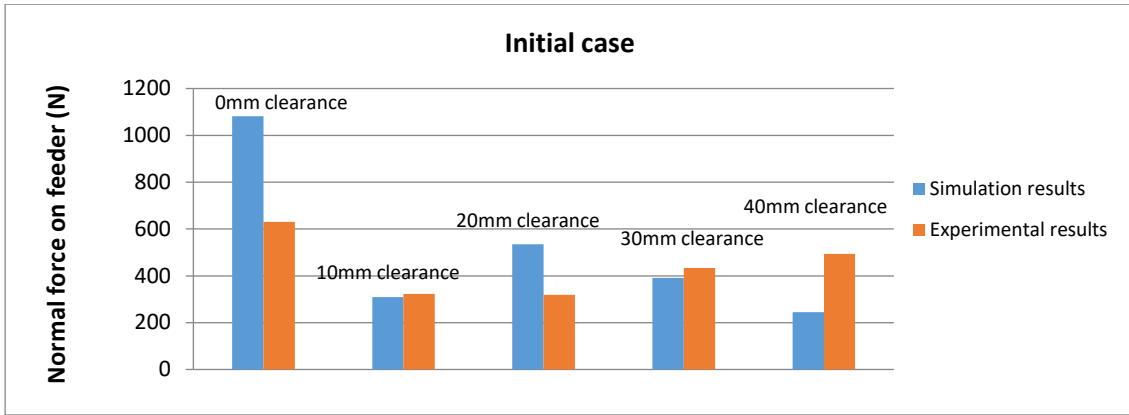


Figure 14: Comparison of the vertical feeder loads at different Clearances for initial condition

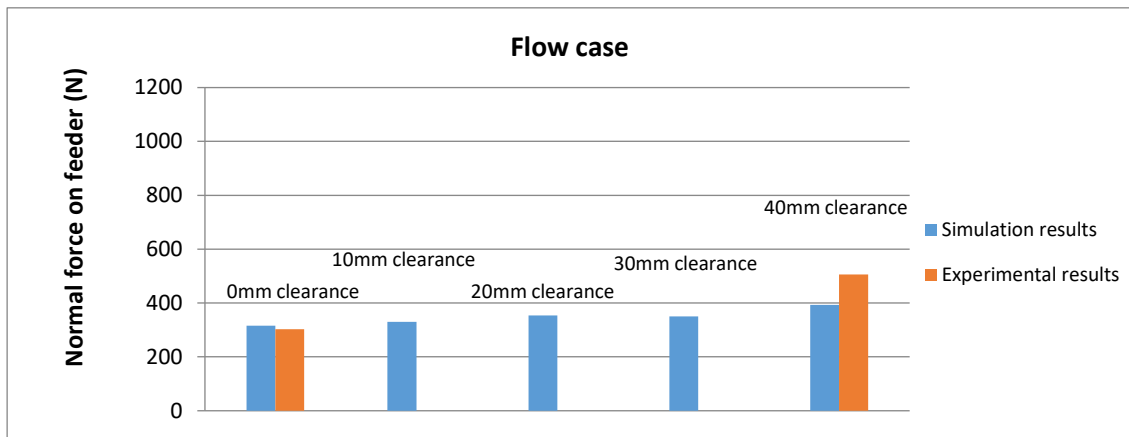


Figure 15: Comparison of the vertical feeder loads at different Clearances for flow condition

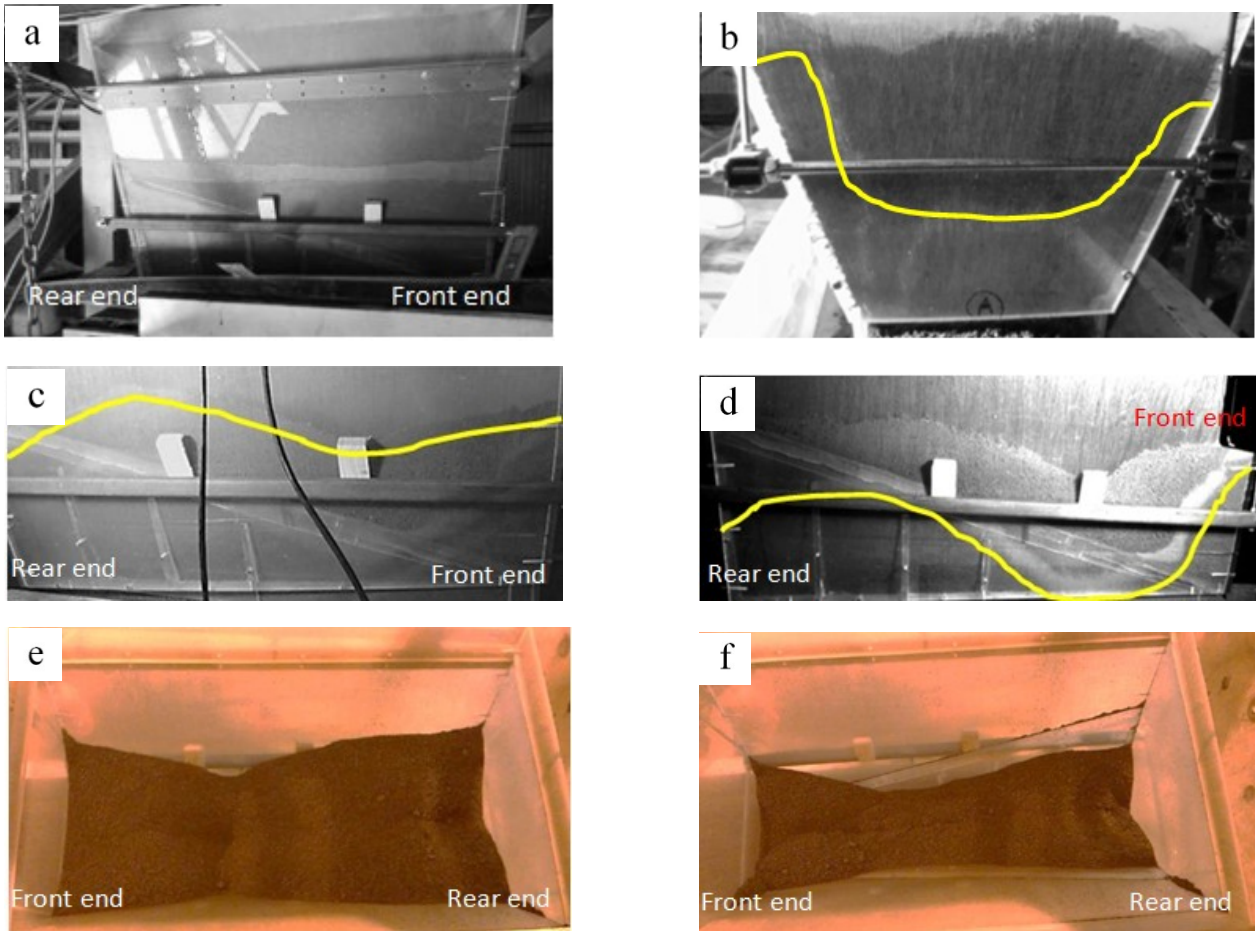


Figure 16: Observed flow patterns: a) Initial position of marked material layer b) 'U' shaped flow pattern at front hopper wall during discharge c) 'S' shaped top surface from side view during discharge d) 'S' shaped flow pattern of marked layer from side view during discharge e) Top view of hopper in the middle of discharge f) Top view of hopper at the end of discharge

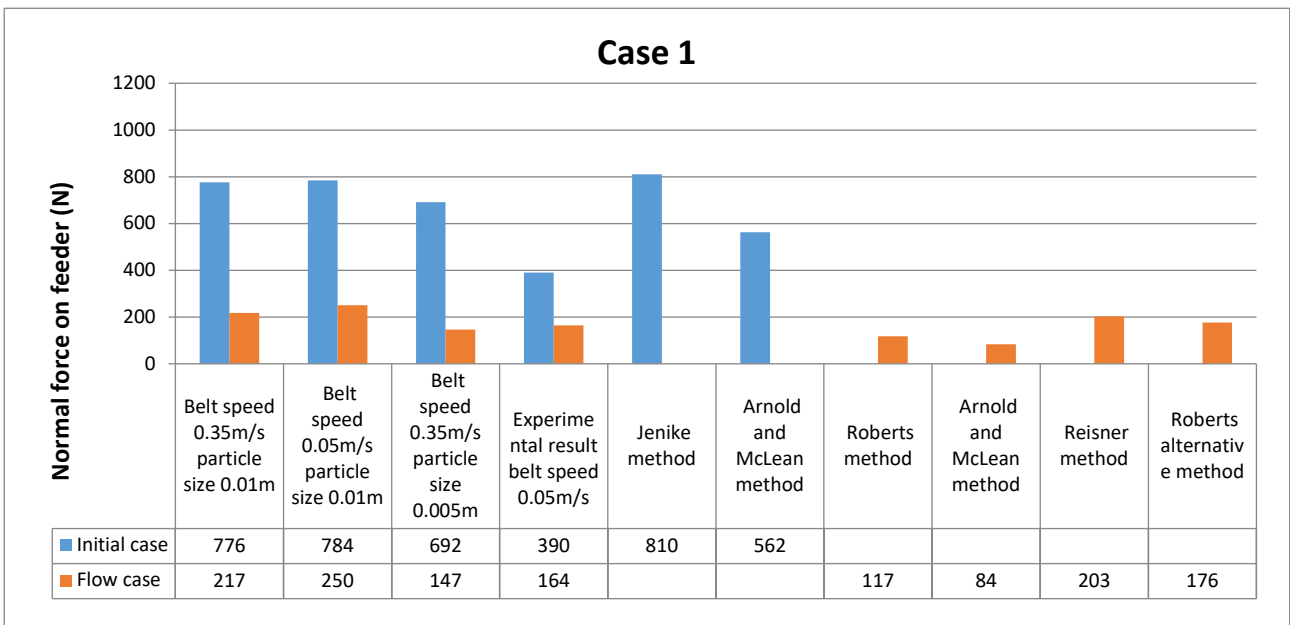


Figure 17 Comparison of the vertical feeder loads at different belt speeds for both initial and flow condition

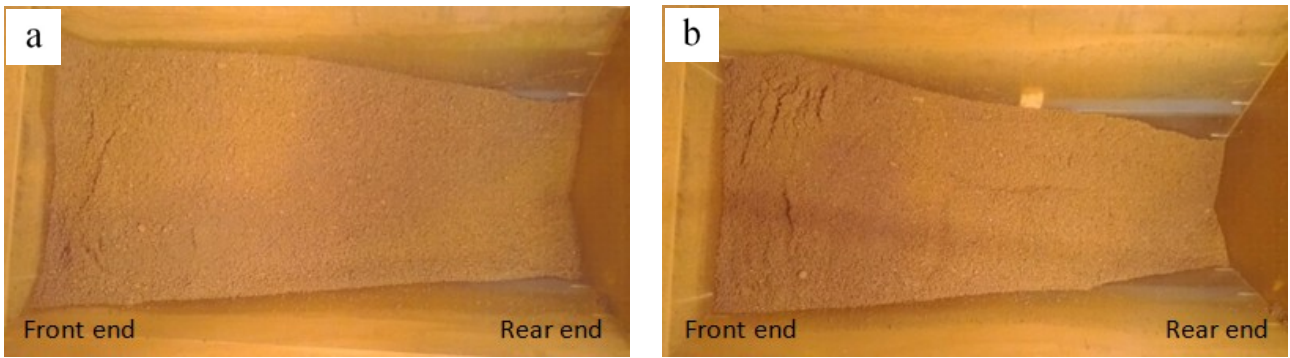


Figure 18: The top view of the flow patterns: a) the earlier time during discharge b) the later time during discharge

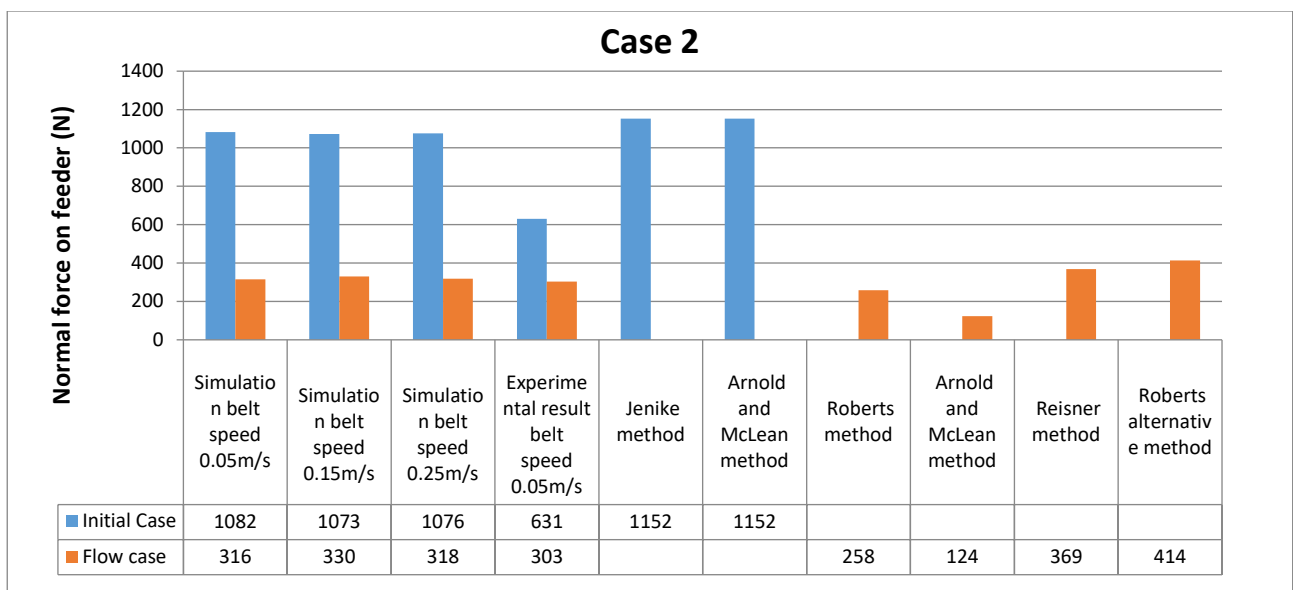


Figure 19: Comparison of the vertical feeder loads at different belt speeds for both initial and flow condition

TABLES

Table 1: Modelling parameters

| Rolling resistance | Particle shape | Particle diameter | Material weight | Particle number | Filling rate | Filling height | Feeder velocity |
|--------------------|----------------|-------------------|-----------------|-----------------|--------------|----------------|-----------------|
| 0.4 | sphere | 0.01m | 200kg | 10,000 | 1000tph | 0.45m | 0.35m/s |